Dielectric permittivity of small-molecule matrices for organic optoelectronics: The key contribution of solid state molecular dynamics

Davide Giavazzi and Anna Painelli
Dipartimento di Scienze Chimiche, della Vita e della Sostenibilità Ambientale, Università di Parma, Parma, Italy

Luca Grisanti*
Division of Theoretical Physics, Ruđer Bošković Institute, Zagreb, Croatia
and National Research Council, Istituto Officina dei Materiali (CNR-IOM)
c/o International School for Advanced Studies (SISSA), Trieste, Italy

Gabriele D'Avino†
Grenoble Alpes University, CNRS, Grenoble INP, Institut Néel, Grenoble 38042, France
and Department of Molecular Sciences and Nanosystems, Ca' Foscari University of Venice, Venice, Italy

(Received 24 September 2025; accepted 7 January 2026; published 2 February 2026)

The dielectric response of amorphous organic solids at the timescale of atomic motion has broad implications for their photophysics, governing spectroscopic properties and excited-state relaxation, among other phenomena. We present an original approach to the calculation of the vibrational contribution to the frequency-dependent dielectric permittivity. Our methodology, combining molecular dynamics simulations, density functional theory calculations, and linear response theory, is applied to a set of amorphous carbazole-based small-molecule matrices, widely used as host materials in organic light-emitting diodes. Our analysis reveals the crucial role of hindered molecular rotations (librations) in the solid-state matrices of dipolar compounds. These modes manifest in the very-low frequency (<100 cm^{-1}) region of the dielectric function, accounting for up to one-third of the total vibrational contribution to the static dielectric constant in a dipolar compound like 3,3'-di(carbazol-9-yl)-5-cyano-1,1'-biphenyl. This low-frequency contribution is found to be crucial for determining the variations in the static dielectric constant across various materials.

DOI: 10.1103/fc1j-sp6w

I. INTRODUCTION

The dielectric permittivity of the active material crucially affects the performance of any optoelectronic device, including those based on organic semiconductors, like organic light-emitting diodes (OLEDs) [1–6] or organic solar cells [7–9]. Key phenomena, such as charge injection and extraction, charge separation, and recombination processes are clearly governed by the ability of the medium to screen Coulomb forces, i.e., by its dielectric response. In OLEDs, Forrest and co-workers have early introduced the concept of solid-state solvation [10,11] to address the dependence of the color of the emitted light on the dielectric properties of the host matrix. More recently, the crucial role of the host medium in the complex photophysics of thermally activated delayed fluorescence OLEDs has been discussed by several groups [2–6,12–15].

The dielectric response of a medium has a distinct dependence on the frequency. In liquid solvents and, more generally in optically transparent organic media, the dielectric response is almost constant in the visible region. Its value, corresponding to the squared refractive index (typically measured at the frequency of the Na yellow line), is a measure of the electronic polarizability of the medium. At lower frequency, vibrational, conformational, and rotational/librational motions contribute to the dielectric response, all contributions summing up in the static dielectric permittivity, the so-called dielectric constant. Organic amorphous media, liquid solvents, polymers, and amorphous matrices made of small molecules typically have similar refractive indices ranging from 1.5 to 2, and dielectric permittivity at optical frequencies in the range 2–4 [16].

In liquid organic solvents with low viscosity, molecules are almost free to tumble around and, in polar solvents (i.e., solvents constituted by polar molecules) this orientational motion gives very large contributions to the dielectric constant. Just as an example, the dielectric constant varies from ∼2 in nonpolar cyclohexane to ∼47 in the strongly polar dimethyl sulphoxide. In dense viscous media, the orientational motion is hindered and it is hard to find materials with very large dielectric constants [17,18]. However, it is not just the value

*Contact author: grisanti@iom.cnr.it
†Contact author: gabriele.davino@unive.it

of the static dielectric constant that matters in defining the properties of a medium; the dielectric dynamics also plays a prominent role. As for liquid nonviscous solvents, relaxation dynamics is very fast, typically in the picosecond timescale [19,20]. Quite extensive studies are available about the dielectric dynamics of polymers [17,21], but little is known about amorphous matrices grown from small molecules (in short, small molecule matrices, SMMs). These matrices are of special interest for OLEDs that are typically fabricated by vapor-phase deposition.

The refractive indexes of common SMMs are easily retrieved, but experimental data on their static dielectric constant are scanty and sometimes controversial [22–24], and even less is known on the frequency dependence of the dielectric response. Recently, attention to this delicate topic has been drawn by de Vries and Coehoorn [25] who proposed a computational approach to estimate the vibrational contribution to the dielectric response. Their approach is simple and computationally effective. For each material, a routine density functional theory (DFT) calculation on the isolated, gas phase-molecule gives access to the frequency and oscillator strength of molecular vibrations, as needed to estimate the vibrational contribution to the dielectric constant. As pointed out in the original paper, the approach relies on several approximations. The harmonic treatment of vibrations, while reasonable for high-frequency modes, is less suitable for low-frequency conformational modes. Furthermore, environmental effects can be significant: gas-phase results may not accurately represent the behavior of amorphous solids because conformational modes are largely hindered in dense media. Moreover, the gas-phase vibrational analysis neglects molecular rotations, which provide the leading contribution to the dielectric constant of liquid polar solvents. In dense SMMs, these motions are largely hindered but not entirely suppressed. A sizable contribution from molecular *librations* is therefore expected, particularly for SMMs made of polar compounds, though this effect remains unexplored.

In this paper, we propose an alternative approach to the calculation of the dielectric constant of a SMM, in an effort to overcome some of the limitations of the original de Vries and Coehoorn approach [25]. Our strategy combines DFT calculations on isolated molecules with classical molecular dynamics (MD) simulations of typical OLED host materials [26,27] and linear response theory [28–31]. We simulate equilibrium trajectories of bulk SMM samples to compute the dipole time-autocorrelation function, from which we obtain the real and imaginary parts of the frequency-dependent susceptibility. The methodology is presented in detail in the Sec. IV at the end of the paper. Our analysis is performed on three carbazole-based SMMs, namely, 4,4'-Bis(carbazol-9-yl)biphenyl (pCBP, also known as CBP), 3,3'-Di(9H-carbazol-9-yl)-1,1'-biphenyl (mCBP), and 3,3'-di(carbazol-9-yl)-5-cyano-1,1'-biphenyl (mCBP-CN) shown in Fig. 1(a). This selection is motivated by crucial structural differences among compounds of similar chemical nature. Specifically, pCBP and mCBP are two isomers with linear and bent shape, respectively, corresponding to a virtually nonpolar and a slightly polar equilibrium structure. The molecular dipole is further enhanced in mCBP-CN, due to the presence of a cyano group.

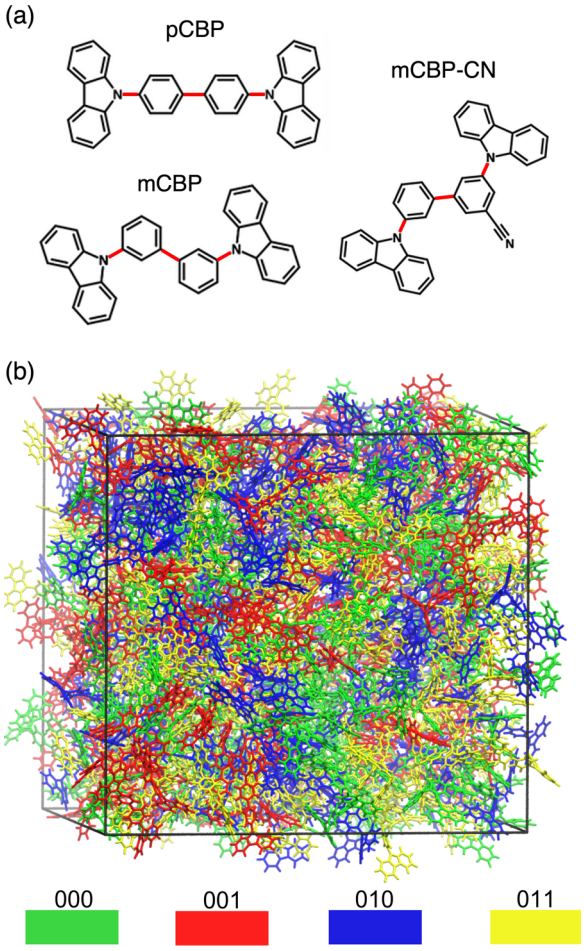

FIG. 1. (a) Molecular structures of the three investigated compounds. Soft inter-ring torsion, giving rise to different stable molecular conformations are highlighted in red. (b) Snapshot extracted from a MD trajectory of a pCBP SMM sample, as an example of investigated systems. Black lines trace the simulation box, containing 512 molecules. Each molecule is colored based on the conformation among the four possible pairs, as shown in the legend at the bottom. See text and the SM [32].

II. RESULTS

A. Dielectric constants from molecular DFT calculations

We start our presentation from an analysis of the vibrational contribution to the dielectric constant ($\varepsilon_{\mathrm{vib}}$) based on gas-phase DFT calculations, extending the methodology proposed by de Vries and Coehoorn [25] to account for the presence of different conformers (see Sec. IV for details). The polycyclic aromatic hydrocarbons under scrutiny indeed feature multiple stable conformations, with distinct inter-ring torsional geometries, as also briefly mentioned in Ref. [25]. The bonds associated to inter-ring torsions are highlighted in red in Fig. 1(a). Possible conformers were identified and labeled according to the methodology presented in the Supplemental Material (SM) [32], Fig. S1. For the sake of illustration, Fig. 1(b) provides a visual rendering of a bulk pCBP sample where the four different conformers have been drawn with different colors.

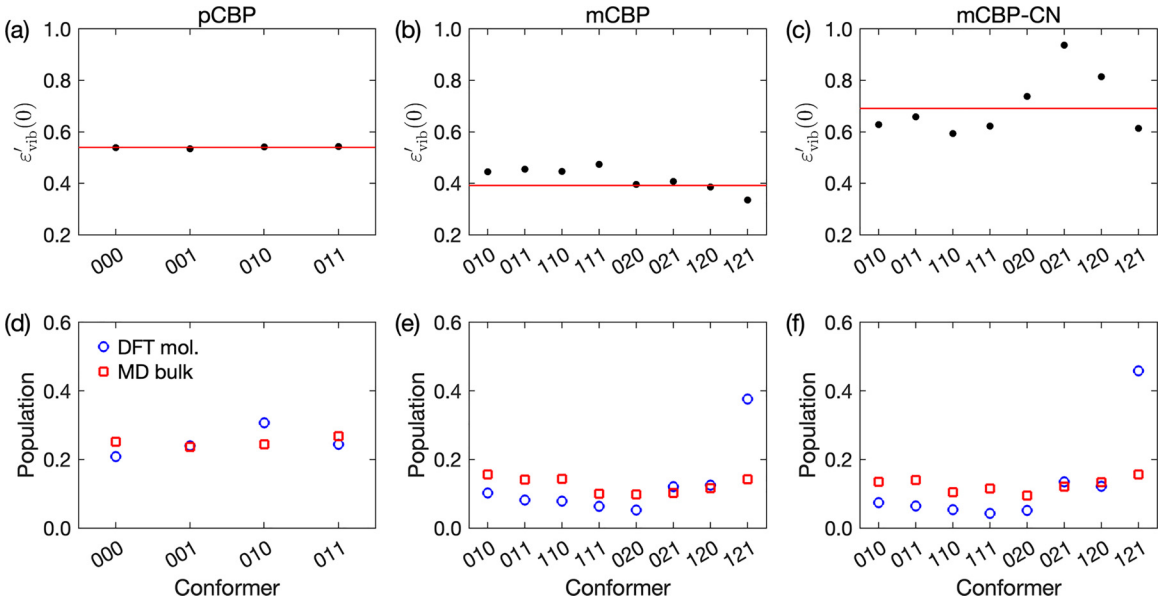

FIG. 2. Vibrational contribution to the static dielectric constant, $\varepsilon'_{\rm vib}(0)$, from gas-phase DFT normal mode calculations. (a)–(c) $\varepsilon'_{\rm vib}(0)$ for the different conformers of pCBP, mCBP, and mCBP-CN (dots) and 300 K Boltzmann average over conformers (red line) based on DFT gas-phase energies. The thermal averages obtained using the conformer populations from solid-state MD simulations are similar and amount to 0.54, 0.42, and 0.70 for pCBP, mCBP, and mCBP-CN, respectively. (d)–(f) Conformer populations obtained from gas-phase DFT energies (Boltzmann statistics, blue circles) and from solid-state MD simulations (red squares).

Figures 2(a)–2(c) show, for the three compounds of interest, the static dielectric constant $\varepsilon'_{\rm vib}(0)$ calculated at the gas-phase DFT level for each conformer. For the nonpolar pCBP molecule, $\varepsilon'_{\rm vib}(0)$ marginally varies with the conformation, while mCBP and to a larger extent mCBP-CN show an important dependence of $\varepsilon_{\rm vib}(0)$ on the conformer. Specifically, in mCBP-CN an ∼50% variability of $\varepsilon'_{\rm vib}(0)$ is observed. The two polar molecules, mCBP and mCBP-CN, differ only due to the presence of a cyano group [see Fig. 1(a)], a seemingly small structural feature that, however, determines an increase of $\varepsilon'_{\rm vib}(0)$ from 0.4 to 0.7 (average over conformers).

In this DFT-based approach, $\varepsilon'_{\rm vib}(0)$ is obtained summing up the contributions from all normal modes, each contribution being proportional to the IR intensity of the mode. In other terms, each mode that modulates the molecular dipole moment contributes to the static dielectric constant. The frequency-resolved analysis in Fig. 3 reveals that a relevant fraction of the susceptibility arises from modes with frequencies above 200 $\rm cm^{-1}$. This contribution to $\varepsilon'_{\rm vib}(0)$ is approximately 0.25, and is very similar for all compounds and conformers. High-frequency modes are typically associated with stretching and bending motions, whose frequency and absorption intensity are marginally affected by the molecular conformation associated with the soft degrees of freedom. On the other hand, the contribution to the dielectric response from modes below 200 $\rm cm^{-1}$, associated to soft flexural and inter-ring torsional degrees of freedom, is strongly affected by the conformation. The contribution of these low-frequency modes also determines the differences between the $\varepsilon'_{\rm vib}(0)$ of the three compounds in the present gas-phase analysis. It is instructive in this respect to compare mCBP and mCBP-CN that only differ for a cyano group. The stretching of the cyano group appears as an intense band at ∼2370 $\rm cm^{-1}$ that only

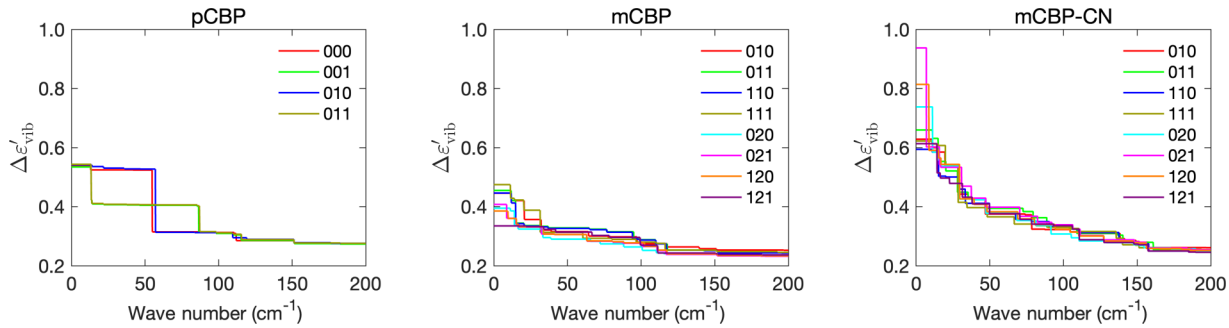

FIG. 3. Frequency-resolved contribution to the static dielectric constant for the possible conformers of the three compounds, obtained from gas-phase DFT calculations. $\Delta\varepsilon'_{\rm vib}(\omega)$ corresponds to the contribution to $\varepsilon'_{\rm vib}(0)$ by all modes with frequency $\geqslant\omega$ [see Eq. (5) in the Sec. IV].

marginally contributes to $\varepsilon'_{\rm vib}(0)$. However, the presence of the cyano group strongly affects the low-frequency contribution to the dielectric constant. The almost twofold increase in $\varepsilon_{\rm vib}(0)$ when going from mCBP to mCBP-CN is hence ascribed to the modulation of the molecular dipole as due to the soft, flexural and torsional modes involving the largely polar cyano group.

Since a distinct $\varepsilon'_{\rm vib}(0)$ can be computed for each stable conformer through harmonic vibrational analysis, an averaging procedure is necessary to obtain a representative value for each compound. DFT energies suggest that the different conformers are thermally accessible (see SM, Table S1), so that sizable populations are expected for all isomers. The red lines in Figs. 2(a)–2(c) show the $\varepsilon'_{\rm vib}(0)$ values calculated for the three compounds as the room-temperature Boltzmann average based on the gas-phase DFT energies of the different conformers. The DFT conformer populations are shown in Figs. 2(d)–2(f) as blue circles, together with the populations obtained from a statistical analysis over the MD equilibrium trajectory at 300 K (red squares; see Sec. IV for details). This comparison shows that the solid-state MD analysis yields nearly equiprobable conformer populations for all systems, while the gas-phase DFT results mark a large prevalence of conformer 121 in both mCBP and mCBP-CN. In this conformer, the carbazole units are in *cis* configuration with respect to the central biphenyl unit, the structure being stabilized by the π stacking interaction between the two face-to-face carbazoles. In the solid state, π-π interactions can also be established with the neighboring molecules, resolving the possible preponderance of a specific conformation. More generally, the qualitative discrepancy between gas and solid-state populations, illustrates the possible pitfalls of a conformational average based on isolated-molecule energies, especially for floppy molecules such as those employed as host in OLEDs.

The gas-phase DFT treatment relying on the harmonic approximation allows for an easy identification of the vibrational modes that mainly contribute to the static dielectric constant (see SM, Table S2 and Figs. S2–S4). However, the approach has some limitations. In the first place, the gas-phase normal modes analysis does not account for molecular rotations, whose contribution typically dominates the dielectric constants of polar molecules in gas or liquid phase. Molecular librations or impeded rotations around an equilibrium occur in amorphous solids, and it is important to evaluate their contribution to the dielectric constant. Second, the harmonic approximation hardly applies to the large-amplitude motions characterizing the low-frequency region of soft molecular systems (e.g., inter-ring torsional dynamics), where the mode mixing and short phonon lifetimes are common phenomena. Importantly, the gas-phase treatment neglects the contribution of intermolecular interactions that have a significant impact on the crucial low-frequency region of the vibrational spectrum and on the conformers populations. Finally, the gas-phase analysis relies on a Clausius-Mossotti treatment of local field effects (see Sec. IV), which might oversimplify the relationship between the molecular and the bulk polarization in complex SMMs.

B. Dielectric function from molecular dynamics

To overcome the limitations of the gas-phase harmonic treatment, we propose an alternative approach to the calculation of the dielectric function of amorphous matrices based on MD simulations and linear response theory. The full methodology is described in the Sec. IV. In a nutshell, large amorphous samples of the three compounds (512 molecules) are built, in order to compute the dielectric function $\varepsilon(\omega)$ from the equilibrium fluctuations of the dipole moment of the sample. The imaginary part of the dielectric function, $\varepsilon''_{\rm vib}(\omega)$, is computed as the Fourier transform of the dipole autocorrelation function. The desired real component of the dielectric function, $\varepsilon'_{\rm vib}(\omega)$ is obtained from the Kramers-Kroning transform of the imaginary part. Due to the large system size and stringent sampling requirements, a first-principles simulation of the amorphous samples at relevant timescales remains computationally prohibitive. We thus opt for classical MD, relying on an atomistic force field (FF) explicitly parametrized for solid-phase simulations of OLED materials [33]. This approach is expected to provide a reliable description of the critical low-frequency spectral region, accounting for intermolecular interactions in the solid state and anharmonicity. Furthermore, ensemble averages performed on equilibrium MD trajectories automatically account for the statistics over the possible molecular conformations.

To assess the reliability of the MD-based methodology, we have first compared the dielectric function of SMMs calculated by sampling the vibrational motion with MD and DFT calculations, both performed in the gas phase. Figure 4 compares the real and imaginary parts of $\varepsilon_{\rm vib}(\omega)$ from gas-phase DFT and MD simulations in the NVE ensemble. In the high-frequency region (above $\sim$900 cm^{-1}, shaded regions) the comparison between DFT and MD reveals significant discrepancies in the frequencies of the IR-active modes, corresponding to the peaks in the $\varepsilon''_{\rm vib}(\omega)$ spectra. In this region, reference DFT results predict a series of intense absorption peaks between 1200 and 1700 cm^{-1} for the three compounds [see Figs. 4(b), 4(d), and 4(f)]. Conversely, MD simulations feature two absorption windows: one at 900–1200 cm^{-1} and the second at 1700–1900 cm^{-1}.

Discrepancies in the high-frequency range are actually not surprising, since the FF provides only a crude approximation of the force constants for the stretching and bending modes of these conjugated systems. In spite of this discrepancy, MD simulations reliably describe the total absorption cross section (IR intensity) of the high-frequency vibrations in the three molecules. This can be inferred from the good match of the baseline of $\varepsilon'_{\rm vib}(\omega)$ below 900 cm^{-1} [see Figs. 4(a), 4(c), and 4(e)]. In this region, dominated by a strong absorption centered at 750 cm^{-1}, a satisfactory agreement is obtained between DFT and MD.

We note a major difference between DFT and MD in the very-low frequency region below 50 cm^{-1}, particularly evident for mCBP-CN. MD simulations for mCBP-CN prescribe a growing tail in $\varepsilon''_{\rm vib}(\omega)$, which arises from molecular free rotations largely modulating the dipole moment [see insets in Figs. 4(e) and 4(f)]. This low-frequency absorption tail in the static $\varepsilon''_{\rm vib}(0)$ is absent in the nonpolar pCBP and much less intense in the weakly polar mCBP [see insets in Figs. 4(a) and 4(c)]. The very-low frequency window is silent in DFT results.

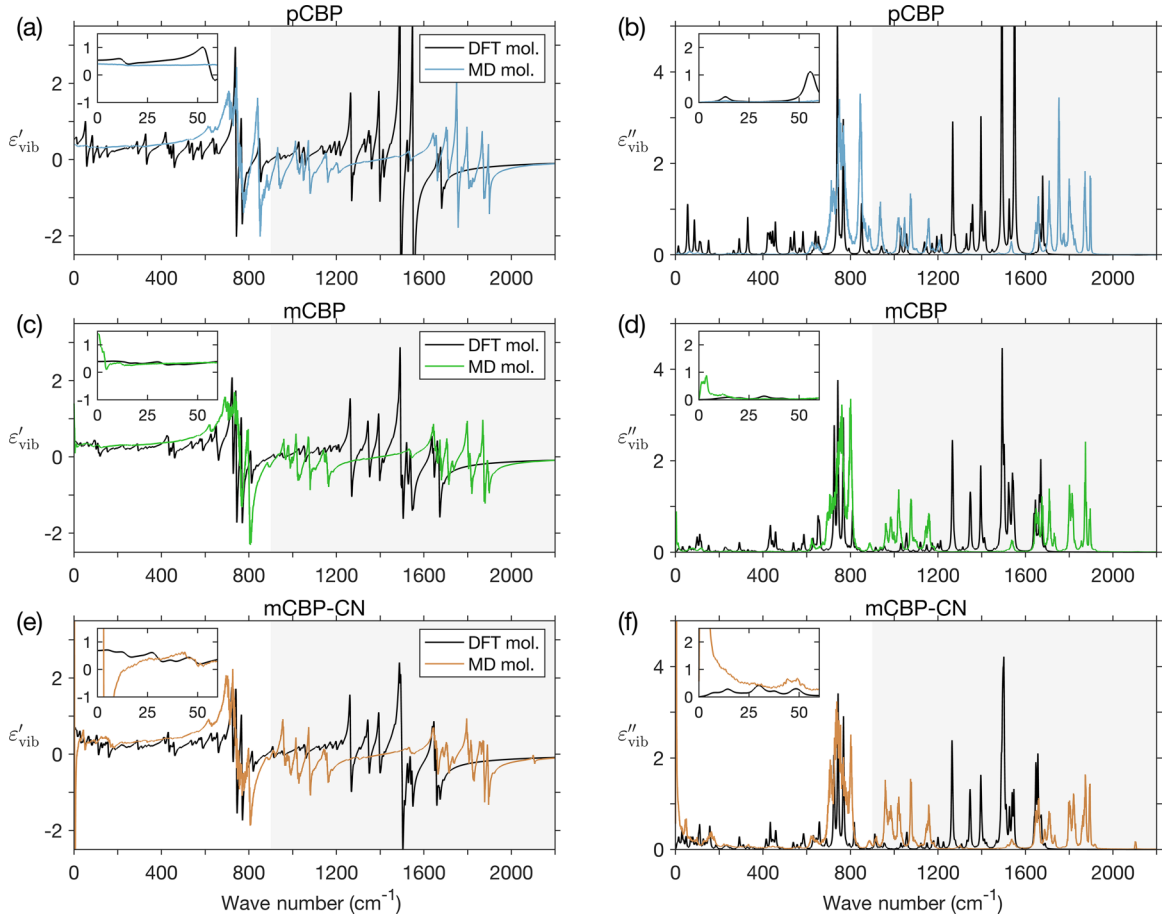

FIG. 4. Real (left) and imaginary (right) parts of the dielectric function of SMMs calculated from gas-phase DFT calculations (Boltzmann average over conformers, black lines) and classical MD simulations on a single molecule (colored lines). Besides some nonsurprising spectral shifts mostly in the high-frequency region (gray shaded area), the favorable comparison between the two methods supports the use of MD for the calculation of the dielectric properties of solid samples.

Indeed, in DFT, as in other first-principles approaches to harmonic molecular vibrations, rigid-body rotations are projected out of the Hessian matrix by applying Eckart conditions. In other words, standard gas-phase DFT calculations completely miss the primary contribution from molecular rotations. This raises concerns about the reliability of this approach for calculating the dielectric properties of solid samples, where the librations of polar molecules can provide a significant contribution.

Having assessed the accuracy of the MD-based methodology on isolated-molecule calculations in the medium- and low-frequency range, we can now discuss the vibrational contribution to the dielectric susceptibility in bulk amorphous solids of interest for organic optoelectronics. Figure 5 shows the real and imaginary parts of the dielectric function for pCBP, mCBP, and mCBP-CN, comparing MD results obtained from gas- and solid-phase simulations. The two simulations lead to very similar $\varepsilon_{\rm vib}(\omega)$ spectra at frequencies above 200 cm^{-1}. This attests that intermolecular interactions in the condensed phase marginally affect high-frequency vibrations with a dominant intramolecular character, as expected.

The dielectric functions of the gas and solid phase remain very similar down to the static limit for the nonpolar compound pCBP [see Figs. 5(a) and 5(b)]. Conversely, for the dipolar compounds, and especially in mCBP-CN, $\varepsilon_{\rm vib}(\omega)$ obtained from isolated-molecule and bulk-sample MD simulations significantly differ below 200 cm^{-1}. As discussed above, molecules undergo free rotations in the gas phase, providing the leading contribution to the static dielectric constant in polar molecules. Molecular rotations are largely hindered in the crowded molecular environment of a SMM; however, a sizable absorption intensity persists as frequencies approach zero in solid mCBP-CN [see $\varepsilon''_{\rm vib}(\omega)$ in Fig. 5(f)]. A finite $\varepsilon''_{\rm vib}(\omega)$ for $\omega < 100$ cm^{-1} is also computed for mCBP [see Fig. 5(d)], although this is barely appreciable on the scale of the figure. In the solid matrix, these very-low frequency absorptions arising from molecular librations control the real part of the dielectric function approaching the static limit, as we shall discuss in the following.

C. Low-frequency MD + DFT dielectric function

DFT calculations have superior accuracy to MD simulations in the high-frequency region that is marginally affected by solid-state interactions (see Fig. 5). On the other hand, the harmonic isolated-molecule DFT treatment of vibrations becomes questionable for thermal vibrations

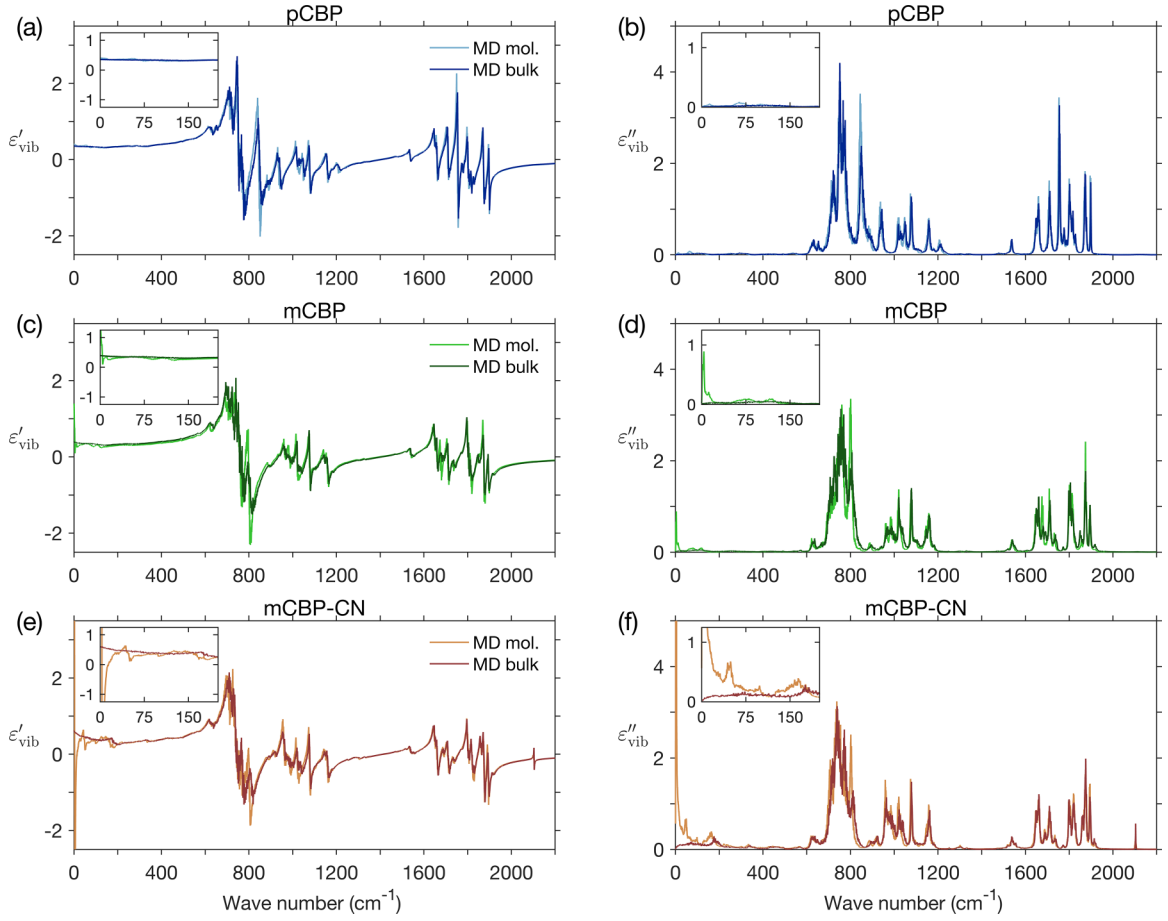

FIG. 5. Dielectric function calculated from isolated-molecule and bulk-solid MD simulations. The inset in each panel provides a zoom of the low-frequency region. Molecular and solid-state simulations yield similar results for $\varepsilon_{\rm vib}(\omega)$ for the three systems, except for the low-frequency region of polar molecules. As is particularly evident for mCBP-CN [panels (e) and (f)], the strong low-frequency absorption in $\varepsilon''_{\rm vib}(\omega)$ due to free rotations in the gas phase is suppressed in the bulk solid. However, libration modes give a finite absorption intensity down to vanishing frequency and a sizable contribution to $\varepsilon'_{\rm vib}(0)$.

in the solid and, importantly, it completely misses the crucial contribution from molecular librations. Librations, conformational disorder, and condensed-phase interactions are instead fully captured in the MD analysis. In order to take the best from both methodologies, we have empirically combined the results of gas-phase DFT calculations and solid-state MD simulations, to obtain a new MD + DFT dielectric function (see Sec. IV for details). In a nutshell, MD and DFT calculations respectively determine the low- and high-frequency regions of the dielectric function. The real part of $\varepsilon_{\rm vib}(\omega)$ coincides with the DFT susceptibility at high frequency and follows the trend of the MD one at low frequency, but with an offset that compensates for the inaccuracy of the FF on the high-frequency modes. Real and imaginary parts of the dielectric function obtained with the MD, DFT, and MD + DFT methods for the three compounds are shown in the SM [32], Fig. S11. Figure 6 provides a low-frequency zoom of the real part of the dielectric function for pCBP, mCBP, and mCBP-CN, as obtained from the combined MD + DFT approach. We first emphasize that the low-frequency behavior is crucial for determining the material-to-material variations in the static dielectric constant, considering the little variations in the contributions of higher-frequency vibrations and electronic degrees of freedom across organic molecular materials. For pCBP $\varepsilon'_{\rm vib}(\omega)$ is almost constant below 150 cm^{-1}, attaining a static limit of $\varepsilon'_{\rm vib}(0) = 0.32$. This confirms the absence of vibrational absorption with appreciable intensity in this spectral window for this system. The dielectric function of mCBP features a plateau ($\varepsilon'_{\rm vib} = 0.26$) between 40 and 80 cm^{-1}, followed by a rising tail at lower frequencies leading to $\varepsilon'_{\rm vib}(0) = 0.32$. This increase, which contributes about 20% to the static $\varepsilon'_{\rm vib}$, can be ascribed to the absorption intensity of libration modes of the weakly polar mCBP, which are IR silent in the nonpolar pCBP. Molecular librations have a much more prominent effect in the strongly polar mCBP-CN, determining a low-frequency tail below 100 cm^{-1} in $\varepsilon'_{\rm vib}(\omega)$, ultimately reaching a static limit $\varepsilon'_{\rm vib}(0) = 0.52$. In the spectrum of mCBP-CN we observe a sizable contribution to $\varepsilon'_{\rm vib}(0)$ due to an absorption feature centered around 180 cm^{-1}. This can be ascribed to an effective dipole modulation by flexural modes in the presence of the strongly polar CN group. Evidence of a large IR intensity around 180 cm^{-1} can also be found in gas-phase DFT and MD calculations confirming its intramolecular origin. Most importantly, we remark that impeded rotations in solid samples composed by polar molecules are responsible

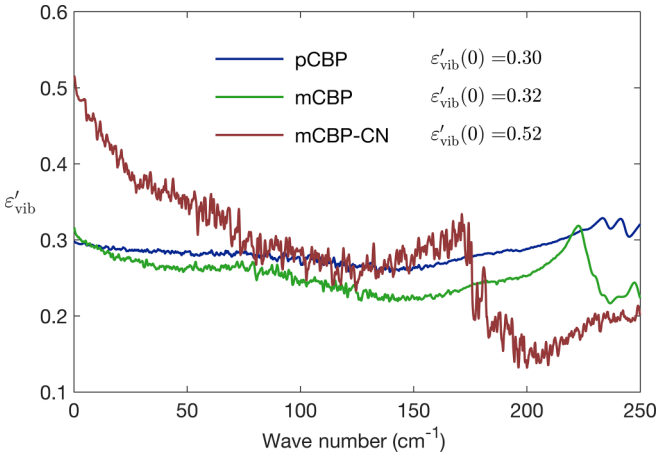

FIG. 6. Comparison of the low-frequency dielectric susceptibility $\varepsilon'_{\rm vib}(\omega)$ for the three investigated solid-state systems, as computed with the combined MF + DFT approach (see Sec. IV and SM Fig. S11 for $\varepsilon''_{\rm vib}(\omega)$ [32]). This highlights the crucial differences arising from low-frequency libration modes in the polar molecule mCBP-CN, determining a large increase in the static dielectric constant $\varepsilon'_{\rm vib}(0)$ over the weakly polar mCBP and the nonpolar pCBP.

for a large fraction of the vibrational contribution to the dielectric constant. In our case, the functionalization of mCBP with a highly polar nitrile group determines a 62% enhancement of $\varepsilon'_{\rm vib}(0)$. On the methodological side, we note that the contribution from molecular librations can only be captured and quantified with a computational approach that explicitly considers the vibrational dynamics of realistic solid-state morphologies, such as large-scale MD simulations in the present study, and it is systematically missed in methods based on isolated molecule calculations.

III. DISCUSSION AND CONCLUSION

In this paper, we have reported an original approach to the calculation of the vibrational contribution to the frequency-dependent dielectric permittivity and its application to a set of amorphous conjugated materials of interest for applications in organic optoelectronics. Albeit the dielectric response at the timescales of the atomic motion has broad implications on different fundamental phenomena of interests for optoelectronic applications, this subject has received little attention from both an experimental and a simulation perspective. In an effort to fill this gap, we have combined MD simulations, DFT calculations, and linear response theory to compute the real and imaginary parts of the dielectric function, accounting for conformational averaging, anharmonicity, and intermolecular interactions in the solid state. Our main finding is that molecular rotations, which typically represent the leading contribution to the dielectric constant in the liquid phases of dipolar molecules, are sterically hindered and mixed with intramolecular and translational modes in the solid state, but definitely they are not silent in the dielectric response. Indeed, our analysis demonstrates that very-low frequency ($<$100 cm^{-1}) librational modes account for approximately 40% of the total vibrational contribution to the static dielectric constant for a polar molecule such as mCBP-CN. These low-frequency modes are found to be crucial for determining the variations in the static dielectric constant across the organic materials considered in this study and likely for other small-molecule matrices.

A direct comparison between our results and experiments is hindered by the paucity of experimental data on the static dielectric constant of organic small-molecule matrices. Experimental data for the electronic and static dielectric constants are only available for pCBP (or CBP) among the studied compounds, suggesting a very small ($<$0.1) vibrational contribution [22,23,34]. This contrasts with our result based on the most accurate MD + DFT method, $\varepsilon_{\rm vib} \sim 0.30$, as well as with that by de Vries and Coehoorn [25], $\varepsilon_{\rm vib} \sim 0.57$. In spite of accuracy limitations presented by molecular simulations, caution should be taken when comparing different data, especially in molecular glassy samples whose structure is largely determined by kinetics. Indeed, in experiments as well as in simulations, different preparation protocols may translate into distinct structural organization and thermodynamic stability, with possibly dramatic impacts on the dielectric properties as well as on photophysics [35]. For instance, a variability in the experimental static dielectric constants up to 0.5 has been reported for common compounds such as N,N′-Di(1-naphthyl)-N,N′-diphenyl-(1,1′-biphenyl)-4,4′-diamine (NPB) [22,23,36–38] and Tris(8-hydroxyquinolinato)aluminium (Alq_3) [23,36,39]. We hope that the present study will stimulate accurate experimental measurements of the optical and static dielectric constants performed on samples prepared according to controlled experimental protocols, in order to clarify the relationship between molecular structure and materials dielectric properties.

A comparison between our results and gas-phase DFT calculations in Ref. [25] is possible for pCBP and mCBP. This reveals an excellent agreement when the modes below 10 meV are excluded from the analysis, which is a direct consequence of the fact that, in our joint MD + DFT approach, the contribution from high-frequency modes is evaluated at a DFT level of theory consistent with Ref. [25]. We, however, stress that harmonic gas-phase DFT calculations are not reliable for the critical low-frequency region of solid-state samples of floppy organic molecules that are heavily influenced by intermolecular interactions and conformational effects. Most importantly, standard gas-phase *ab initio* analyses completely miss the leading contribution of molecular librations in polar molecules, representing a qualitatively novel effect that can only be captured by methodologies that explicitly account for intermolecular solid-state phenomena.

Detailed information is available about the dielectric dynamics in common nonviscous liquid solvents, in which the dielectric relaxation is completed in a few picoseconds [19,20]. Much less is known for amorphous molecular solids. Recent time-resolved emission experiments on molecular dyes dispersed in SMMs demonstrate that the dielectric relaxation is not completed in 15 ns [40]. The present study shows that dielectric relaxation of SMMs persists beyond a few hundreds of picoseconds (see SM, Fig. S10), although we could not find evidence for dielectric dynamics beyond the nanosecond timescale, a result consistent with previous MD-

based simulations [27]. The apparent contradiction between our findings and experimental data [40] can be due to several nonexclusive reasons. First, we note that our simulations explicitly target the bulk, macroscopic, dielectric function of pure SMMs, ignoring the presence of a guest specie and the nonlocal nature of the microscopic dielectric response that is relevant for the dye emission. Moreover, the dielectric relaxation following an optical transition is a nonequilibrium phenomenon implying the dissipation of energy from the excited dye to the molecular surroundings. Such a relaxation dissipates energy to the local environment, possibly activating molecular motions differing from the equilibrium dynamics, e.g., by overcoming high-energy activation barriers. The present analysis therefore excludes that the observed slow post-excitation dynamics [40] is a bulk equilibrium phenomenon.

In summary, this work provides molecular dynamics insights into the dielectric properties of SMMs for organic optoelectronic applications, drawing attention to the role of solid-state interactions on the low-frequency dielectric response, and specifically revealing the crucial role of molecular librations. The complex phenomenology of solid-state solvation, however, calls for additional experimental and simulation work to fully understand how optical spectra and excited-state relaxation depend on the structure and dynamics of molecular amorphous matrices.

IV. METHODS

A. Molecular dynamics simulations

Classical MD simulations have been performed to sample the thermal motion of isolated molecules and of amorphous solid-state samples of the three compounds of interest, pCBP, mCBP, and mCBP-CN. We have employed the all-atom FF for solid-phase simulations of OLED materials as developed by Moral *et al.* [33]. This FF, named T-FA in the original paper, is based on the General Amber Force Field (GAFF) [41], complemented with compound-specific atomic charges from electrostatic potential fitting (ESP scheme) [42], a DFT-based reparametrization of the soft inter-ring torsional potentials and the tuning of Lennard-Jones parameters. The T-FA force field was specifically validated against experimental data for a family of chemical systems largely overlapping with those under investigation. Here, in addition, the force field for mCBP-CN has been complemented with parameters for the cyano group taken from the GAFF 2010 [41], but for the C-N stretching force constant (from Tiberio *et al.* [43]) and the corresponding equilibrium distance, computed at the PBE0/def2-SVP level [44–46]. According to the prescriptions of Ref. [33], ESP [42] atomic charges computed at the PBE0/def2-TVZP level of theory have been adopted to describe electrostatic interactions. All MD simulations have been performed with the NAMD 2.12 code [47], employing an integration time step of 0.5 fs and the Langevin thermostats (damping 0.5 ps^{-1}) for constant-temperature dynamics. Nonbonded interactions have been computed within a cutoff distance of 1.2 nm.

Amorphous solid samples have been prepared following a simulation protocol devised in earlier works [48,49], consisting in the progressive compression and equilibration of an initial low-density isotropic sample. Specifically, we set up a box of 8×8×8 randomly oriented molecules placed at the nodes of a cubic lattice (spacing 2.5 nm) that was used as a starting geometry in the following two-step equilibration protocol: (1) NPT run at high pressure (10-100-200 atm) and high temperature (900 K) in order to progressively compress the sample while ensuring an enhanced molecular motion. This run was conducted until a rough energy equilibration (1 to 2 ns), corresponding to sample densities comparable to room-condition ones. (2) NPT equilibration at room temperature (300 K) and pressure (1 atm) for 20 ns. Production runs from 0.6 to 60 ns were then performed on equilibrated samples in order to sample the thermal molecular motion and dipole fluctuations. Solid-state simulations employed the Particle Mesh Ewald algorithm [50] for the evaluation of long-range electrostatic interactions. Pressure control has been implemented with a Berendsen barostat. The convergence of the results with respect to the sample size has been explicitly checked by comparing results obtained for systems with a number of molecules ranging from 6^3 to 8^3, leading to comparable results (see SM, Fig. S5). The MD simulations of isolated molecules have been performed in both the NVT and the NVE ensembles, leading to consistent results (see SM, Fig. S6).

B. Linear response theory

The frequency-dependent relative dielectric function $\varepsilon_{\text{vib}}(\omega)$ is obtained from the fluctuations of dipole moment at thermal equilibrium. The time evolution of the dipole moment of the investigated samples is obtained from the MD trajectories, adopting a point-charge model: $\boldsymbol{\mu}(t) = \sum_k q_k \mathbf{r}_k(t)$, where $\mathbf{r}_k$ and q_k are the position and the charge of atom k, respectively. A proper choice of the atomic charges is essential to obtain reliable values for the dielectric function. Different sets of charges have been tested, leading us to finally opt for the ESP atomic charges [42], as those that best reproduce the DFT molecular dipoles and their geometry dependence (see SM, Figs. S7 and S8). This analysis was performed on 2048 phenyl-carbazole molecules (chosen as a common building block among all the investigated systems) extracted from a MD trajectory of a bulk amorphous sample (see SM, Fig. S9). SM Fig. S7 testifies to the excellent correlation between the Cartesian components of the DFT and FF dipole, as well as a systematic overestimation by 14% of the dipole fluctuations by the FF. The dipole moments calculated with atomic charges have thus been multiplied by a scaling factor of 0.88 for the calculation of the dielectric properties, to match the reference DFT values. Calculations on a limited number of geometries show that the same scaling factor is a representative value for the compounds investigated in this work (see SM, Fig. S8). The scaling factor only affects the dipole post processing, not the calculation of electrostatic interactions within the MD trajectory.

The imaginary part of the permittivity (i.e., the absorption spectrum) is obtained from the Fourier transform of the dipole autocorrelation function (ACF), $\langle \mu(0)\, \mu(t) \rangle$ [28,29], as follows:

$$\varepsilon''_{\text{vib}}(\omega) = \frac{1}{2\hbar\varepsilon_0 V} \frac{\hbar\omega}{k_B T} \int_{-\infty}^{\infty} \langle \mu(0)\mu(t) \rangle e^{-i\omega t} dt, \qquad (1)$$

where V is the sample volume, T the absolute temperature, $\hbar$ the reduced Plank constant, ε_0 the vacuum permittivity, and k_B the Boltzmann constant. ACFs were computed for each Cartesian component of the dipole and then averaged, in line with the isotropic nature of our amorphous samples. Equation (1) includes quantum corrections for harmonic oscillators to the classical ACF, which are needed in order to respect detailed balance and ensure a proper temperature dependence of the absorption spectrum [51–53]. The results presented in the paper have been obtained with ACFs computed using production trajectories of 0.6 ns, sampled at 4 fs time intervals. ACFs have been multiplied by an exponential damping factor with 20 ps time constant so as to smooth the spectra. We have explicitly checked that extending the simulation time to 60 ns and adopting damping factors up to 20 ns does not lead to the emergence of an additional low-frequency signal in $\varepsilon_{\rm vib}(\omega)$ (see SM, Fig. S10). The real part of the dielectric function can finally be calculated as the Kramers-Kronig transform of the absorptive component.

$$\varepsilon'_{\rm vib}(\omega) = -\frac{1}{\pi}\int_{-\infty}^{\infty}\frac{\varepsilon''_{\rm vib}(\omega')}{\omega'-\omega}d\omega', \tag{2}$$

where the integral over the real variable ω' is defined as the Cauchy principal value. The Kramers-Kronig transform has been evaluated numerically using the algorithm provided in Ref. [54].

C. Permittivity calculation from DFT normal modes

The vibrational contribution to the dielectric function has been calculated by combining DFT calculations (isolated molecules, harmonic approximation) with the Lorentz oscillator model. All DFT calculations have been performed in vacuum with the ORCA 5.0.2 package [55], at the PBE0/def2-TZVP level of theory [44–46], using D3-BJ dispersion corrections [56]. Geometries were first optimized with tight convergence criteria, and then employed in the calculation of analytical vibrational frequencies and infrared absorption intensity. Details on the conformational analysis are available in the SM, Fig. S1 and Table S1(see also Refs. [57,58] therein).

The DFT vibrational analysis allows the calculation of the vibrational contribution to the molecular polarizability

$$\alpha_{\rm vib}(\omega) = \frac{n\varepsilon_0}{10N_{\rm A}\pi^2}\sum_j\frac{A_j}{\omega_j^2-\omega^2-i\omega\gamma}, \tag{3}$$

where ω_j and A_j are, respectively, the frequency and the absorption intensity of the jth mode; γ is the damping factor, n is the refractive index of the material, $N_{\rm A}$ is the Avogadro constant, and i is the imaginary unit. The values $\gamma = 5$ cm^{-1} and $n = 1.7$ have been used for all compounds. For frequencies expressed in cm^{-1} and A_j in Km/mol, Eq. (3) yields the molecular polarizability in SI units. The Clausius-Mossotti equation is adopted to account for local fields in polarized condensed media [25], leading to the dielectric function

$$\varepsilon_{\rm vib}(\omega) = \left[\frac{(n^2+2)^2}{9-(n^2+2)N\alpha_{\rm vib}(\omega)/\varepsilon_0}\right]\frac{N\alpha_{\rm vib}(\omega)}{\varepsilon_0}, \tag{4}$$

where $N = \rho N_{\rm A}/M$ is the number density, here calculated from the mass density $\rho = 1.16\times10^3$ Kg/m^3 (from MD simulation, without significative differences between the three systems) and the molar mass M. The vibrational dielectric constant can be obtained as the static limit of Eqs. (3) and (4):

$$\varepsilon_{\rm vib}(0) = \frac{n\varepsilon_0}{10N_{\rm A}\pi^2}\left[\frac{(n^2+2)^2}{9-(n^2+2)N\alpha_{\rm vib}(0)/\varepsilon_0}\right]\sum_j\frac{A_j}{\omega_j^2}. \tag{5}$$

D. Combining MD and DFT permittivities

The dielectric functions calculated with the two techniques are combined to obtain a joint MD + DFT $\varepsilon_{\rm vib}(\omega)$, tracking the dipole fluctuations from MD at low frequency and the high-frequency fluctuations from DFT. The proposed merging is based on the following frequency-based switch between the imaginary parts of the dielectric functions obtained with the two methods:

$$\varepsilon''(\omega) = f(\omega)\varepsilon''_{\rm MD}(\omega) + [1-f(\omega)]\varepsilon''_{\rm DFT}(\omega), \tag{6}$$

where the function $f(\omega) = (e^{(\omega-\omega_{\rm s})/\delta\omega}+1)^{-1}$ goes from 1 to 0 in a frequency window $\delta\omega$ centered at the switch frequency $\omega_{\rm s}$. The real part of the joint MD + DFT dielectric function is then obtained upon Kramers-Kronig transform, Eq. (2).

Equation (6) has a clear physical motivation but is inherently empirical, leaving arbitrariness in the choice of the parameters $\omega_{\rm s}$ and $\delta\omega$. The data presented in the paper have been obtained for $\delta\omega = 10$ cm^{-1} and a system-dependent switch frequency falling in a nonabsorbing region of the MD and DFT spectra, viz., $\omega_{\rm s} = 205$ cm^{-1} for pCBP and mCBP $\omega_{\rm s} = 265$ cm^{-1} for mCBP-CN. We have explicitly checked the robustness of our results on the choice of the two arbitrary parameters in a meaningful range. Specifically, variations in the static dielectric constant $\varepsilon_{\rm vib}(0)$ below 0.01 were found for $\omega_{\rm s}$ in the 200–300 cm^{-1} range and $\delta\omega$ in the 5–20 cm^{-1} range (see SM, Table S3).

ACKNOWLEDGMENTS

The authors acknowledge the contribution of Mattia Anzola in the first steps of this work. This work was partially supported by the "PHC COGITO" programme (call 2023/24, Project No. 49251YB), funded by the French Ministry for Europe and Foreign Affairs, the French Ministry for Higher Education and Research and The Croatian Ministry of Science and Education. G.D. acknowledges support from the French "Agence Nationale de la Recherche," project RAPTORS (ANR-21-CE24-0004-01). Work in Parma was funded by PNRR MUR Project No. ECS-00000033-ECOSISTER, with the support of the local High Performance Computing facility and in the framework of the COMP-R Initiative, funded by the "Departments of Excellence program of the Italian Ministry for University and Research" (MUR).

DATA AVAILABILITY

The data that support the findings of this article are not publicly available upon publication because it is not technically feasible and/or the cost of preparing, depositing, and hosting the data would be prohibitive within the terms of this research project. The data are available from the authors upon reasonable request.

[1] H. Sun, Z. Hu, C. Zhong, X. Chen, Z. Sun, and J.-L. Brédas, Impact of dielectric constant on the singlet–triplet gap in thermally activated delayed fluorescence materials, J. Phys. Chem. Lett. **8**, 2393 (2017).

[2] J.-M. Mewes, Modeling TADF in organic emitters requires a careful consideration of the environment and going beyond the Franck–Condon approximation, Phys. Chem. Chem. Phys. **20**, 12454 (2018).

[3] D. K. A. P. Huu, S. Saseendran, and A. Painelli, Effective models for TADF: the role of the medium polarizability, J. Mater. Chem. C **10**, 4620 (2022).

[4] A. J. Gillett, A. Pershin, R. Pandya, S. Feldmann, A. J. Sneyd, A. M. Alvertis, E. W. Evans, T. H. Thomas, L.-S. Cui, B. H. Drummond, G. D. Scholes, Y. Olivier, A. Rao, R. H. Friend, and D. Beljonne, Dielectric control of reverse intersystem crossing in thermally activated delayed fluorescence emitters, Nat. Mater. **21**, 1150 (2022).

[5] T. Serevičius, R. Skaisgiris, J. Dodonova, I. Fiodorova, K. Genevičius, S. Tumkevičius, K. Kazlauskas, and S. Juršėnas, Temporal dynamics of solid-state thermally activated delayed fluorescence: Disorder or ultraslow solvation? J. Phys. Chem. Lett. **13**, 1839 (2022).

[6] D. K. A. P. Huu, S. Saseendran, R. Dhali, L. G. Franca, K. Stavrou, A. Monkman, and A. Painelli, Thermally activated delayed fluorescence: Polarity, rigidity, and disorder in condensed phases, J. Am. Chem. Soc. **144**, 15211 (2022).

[7] F. Jahani, S. Torabi, R. C. Chiechi, L. J. A. Koster, and J. C. Hummelen, Fullerene derivatives with increased dielectric constants, Chem. Commun. **50**, 10645 (2014).

[8] A. Armin, D. M. Stoltzfus, J. E. Donaghey, A. J. Clulow, R. C. R. Nagiri, P. L. Burn, I. R. Gentle, and P. Meredith, Engineering dielectric constants in organic semiconductors, J. Mater. Chem. C **5**, 3736 (2017).

[9] S. Sami, R. Alessandri, R. Broer, and R. W. A. Havenith, How ethylene glycol chains enhance the dielectric constant of organic semiconductors: Molecular origin and frequency dependence, ACS Appl. Mater. Interfaces **12**, 17783 (2020).

[10] V. Bulović, A. Shoustikov, M. Baldo, E. Bose, V. Kozlov, M. Thompson, and S. Forrest, Bright, saturated, red-to-yellow organic light-emitting devices based on polarization-induced spectral shifts, Chem. Phys. Lett. **287**, 455 (1998).

[11] V. Bulović, R. Deshpande, M. Thompson, and S. Forrest, Tuning the color emission of thin film molecular organic light emitting devices by the solid state solvation effect, Chem. Phys. Lett. **308**, 317 (1999).

[12] G. Méhes, K. Goushi, W. J. Potscavage, and C. Adachi, Influence of host matrix on thermally-activated delayed fluorescence: Effects on emission lifetime, photoluminescence quantum yield, and device performance, Org. Electron. **15**, 2027 (2014).

[13] P. L. dos Santos, J. S. Ward, M. R. Bryce, and A. P. Monkman, Using guest–host interactions to optimize the efficiency of TADF OLEDs, J. Phys. Chem. Lett. **7**, 3341 (2016).

[14] P. K. Samanta, D. Kim, V. Coropceanu, and J.-L. Brédas, Upconversion intersystem crossing rates in organic emitters for thermally activated delayed fluorescence: Impact of the nature of singlet vs triplet excited states, J. Am. Chem. Soc. **139**, 4042 (2017).

[15] K. Stavrou, L. G. Franca, and A. P. Monkman, Photophysics of TADF guest–host systems: Introducing the idea of hosting potential, ACS Appl. Electron. Mater. **2**, 2868 (2020).

[16] S. R. Forrest, *Organic Electronics: Foundations to Applications* (Oxford University Press, Oxford, UK, 2020).

[17] Z. Ahmad, Polymer dielectric materials, *Dielectric Material* (InTech, London 2012).

[18] H. Li, Y. Zhou, Y. Liu, L. Li, Y. Liu, and Q. Wang, Dielectric polymers for high-temperature capacitive energy storage, Chem. Soc. Rev. **50**, 6369 (2021).

[19] E. W. Castner, M. Maroncelli, and G. R. Fleming, Subpicosecond resolution studies of solvation dynamics in polar aprotic and alcohol solvents, J. Chem. Phys. **86**, 1090 (1987).

[20] M. L. Horng, J. A. Gardecki, A. Papazyan, and M. Maroncelli, Subpicosecond measurements of polar solvation dynamics: Coumarin 153 revisited, J. Phys. Chem. **99**, 17311 (1995).

[21] K. Grzybowska, A. Grzybowski, J. Zioło, M. Paluch, and S. Capaccioli, Dielectric secondary relaxations in polypropylene glycols, J. Chem. Phys. **125**, 044904 (2006).

[22] T. Matsushima, G.-H. Jin, Y. Kanai, T. Yokota, S. Kitada, T. Kishi, and H. Murata, Interfacial charge transfer and charge generation in organic electronic devices, Org. Electron. **12**, 520 (2011).

[23] Y. Noguchi, Y. Miyazaki, Y. Tanaka, N. Sato, Y. Nakayama, T. D. Schmidt, W. Brütting, and H. Ishii, Charge accumulation at organic semiconductor interfaces due to a permanent dipole moment and its orientational order in bilayer devices, J. Appl. Phys. **111**, 114508 (2012).

[24] E. Skuodis, O. Bezvikonnyi, A. Tomkeviciene, D. Volyniuk, V. Mimaite, A. Lazauskas, A. Bucinskas, R. Keruckiene, G. Sini, and J. V. Grazulevicius, Aggregation, thermal annealing, and hosting effects on performances of an acridan-based TADF emitter, Org. Electron. **63**, 29 (2018).

[25] X. de Vries and R. Coehoorn, Vibrational mode contribution to the dielectric permittivity of disordered small-molecule organic semiconductors, Phys. Rev. Mater. **4**, 085602 (2020).

[26] Y. Olivier, B. Yurash, L. Muccioli, G. D'Avino, O. Mikhnenko, J. C. Sancho-García, C. Adachi, T.-Q. Nguyen, and D. Beljonne, Nature of the singlet and triplet excitations mediating thermally activated delayed fluorescence, Phys. Rev. Mater. **1**, 075602 (2017).

[27] T. Northey, J. Stacey, and T. J. Penfold, The role of solid state solvation on the charge transfer state of a thermally activated delayed fluorescence emitter, J. Mater. Chem. C **5**, 11001 (2017).

[28] R. Gordon, Correlation functions for molecular motion, in *Advances in Magnetic Resonance*, edited by J. S. Waugh (Academic, New York, 1968), Vol. 3, pp. 1–42.

[29] G. Williams, Use of the dipole correlation function in dielectric relaxation, Chem. Rev. **72**, 55 (1972).

[30] P. L. Silvestrelli, M. Bernasconi, and M. Parrinello, *Ab initio* infrared spectrum of liquid water, Chem. Phys. Lett. **277**, 478 (1997).

[31] F. Pabst and S. Baroni, How salt solvation slows water dynamics while blue-shifting its dielectric spectrum, J. Phys. Chem. Lett. **16**, 7915 (2025).

[32] See Supplemental Material at http://link.aps.org/supplemental/10.1103/fc1j-sp6w for additional methodology details and calcualtion results.

[33] M. Moral, W.-J. Son, J. C. Sancho-García, Y. Olivier, and L. Muccioli, Cost-effective force field tailored for solid-phase simulations of OLED materials, J. Chem. Theory Comput. **11**, 3383 (2015).

[34] Z. Liu, C. Kwong, C. Cheung, A. Djurišić, Y. Chan, and P. Chui, The characterization of the optical functions of BCP and CBP thin films by spectroscopic ellipsometry, Synth. Met. **150**, 159 (2005).

[35] J. Ràfols-Ribé, P.-A. Will, C. Hänisch, M. Gonzalez-Silveira, S. Lenk, J. Rodríguez-Viejo, and S. Reineke, High-performance organic light-emitting diodes comprising ultrastable glass layers, Sci. Adv. **4**, eaar8332 (2018).

[36] S. Berleb, W. Brütting, and G. Paasch, Interfacial charges and electric field distribution in organic hetero-layer light-emitting devices, Org. Electron. **1**, 41 (2000).

[37] Y. Xu, Y. Tao, H. Zhang, X. Chen, G. Cao, Z. Xu, H. Li, S. Bao, and P. He, Impedance spectroscopy study on transport properties of *n*,*n*′-diphenyl-*n*,*n*′-bis(1-naphthyl)-1,1′-biphenyl-4,4′-diamine, Phys. B (Amsterdam, Neth.) **362**, 35 (2005).

[38] S. L. M. van Mensfoort, V. Shabro, R. J. de Vries, R. A. J. Janssen, and R. Coehoorn, Hole transport in the organic small molecule material α-NPD: Evidence for the presence of correlated disorder, J. Appl. Phys. **107**, 113710 (2010).

[39] R. L. Martin, J. D. Kress, I. H. Campbell, and D. L. Smith, Molecular and solid-state properties of tris-(8-hydroxyquinolate)-aluminum, Phys. Rev. B **61**, 15804 (2000).

[40] B. Bardi, D. Giavazzi, E. Ferrari, A. Iagatti, M. Di Donato, D. K. A. P. Huu, F. Di Maiolo, C. Sissa, M. Masino, A. Lapini, and A. Painelli, Solid state solvation: A fresh view, Mater. Horiz. **10**, 4172 (2023).

[41] J. Wang, R. M. Wolf, J. W. Caldwell, P. A. Kollman, and D. A. Case, Development and testing of a general AMBER force field, J. Comput. Chem. **25**, 1157 (2004).

[42] B. H. Besler, K. M. Merz, Jr., and P. A. Kollman, Atomic charges derived from semiempirical methods, J. Comput. Chem. **11**, 431 (1990).

[43] G. Tiberio, L. Muccioli, R. Berardi, and C. Zannoni, Towards *in silico* liquid crystals. Realistic transition temperatures and physical properties for *n*-cyanobiphenyls via molecular dynamics simulations, ChemPhysChem **10**, 125 (2009).

[44] J. P. Perdew, M. Ernzerhof, and K. Burke, Rationale for mixing exact exchange with density functional approximations, J. Chem. Phys. **105**, 9982 (1996).

[45] C. Adamo and V. Barone, Toward reliable density functional methods without adjustable parameters: The PBE0 model, J. Chem. Phys. **110**, 6158 (1999).

[46] F. Weigend and R. Ahlrichs, Balanced basis sets of split valence, triple zeta valence and quadruple zeta valence quality for H to Rn: Design and assessment of accuracy, Phys. Chem. Chem. Phys. **7**, 3297 (2005).

[47] J. C. Phillips, R. Braun, W. Wang, J. Gumbart, E. Tajkhorshid, E. Villa, C. Chipot, R. D. Skeel, L. Kalé, and K. Schulten, Scalable molecular dynamics with NAMD, J. Comput. Chem. **26**, 1781 (2005).

[48] G. D'Avino, Y. Olivier, L. Muccioli, and D. Beljonne, Do charges delocalize over multiple molecules in fullerene derivatives? J. Mater. Chem. C **4**, 3747 (2016).

[49] O. M. Roscioni, M. Ricci, C. Zannoni, and G. D'Avino, Are coarse-grained structures as good as atomistic ones for calculating the electronic properties of organic semiconductors? J. Phys. Chem. C **127**, 9225 (2023).

[50] U. Essmann, L. Perera, M. L. Berkowitz, T. Darden, H. Lee, and L. G. Pedersen, A smooth particle mesh Ewald method, J. Chem. Phys. **103**, 8577 (1995).

[51] S. Valleau, A. Eisfeld, and A. Aspuru-Guzik, On the alternatives for bath correlators and spectral densities from mixed quantum-classical simulations, J. Chem. Phys. **137**, 224103 (2012).

[52] S. A. Egorov, K. F. Everitt, and J. L. Skinner, Quantum dynamics and vibrational relaxation, J. Phys. Chem. A **103**, 9494 (1999).

[53] D. Semrouni, A. Sharma, J.-P. Dognon, G. Ohanessian, and C. Clavaguéra, Finite temperature infrared spectra from polarizable molecular dynamics simulations, J. Chem. Theory Comput. **10**, 3190 (2014).

[54] V. Lucarini, J. J. Saarinen, K.-E. Peiponen, and E. M. Vartiainen, *Kramers-Kronig Relations in Optical Materials Research*, Springer Series in Optical Sciences Vol. 110 (Springer-Verlag, Berlin, Heidelberg, 2005).

[55] F. Neese, Software update: The orca program system—version 5.0, WIREs Comput. Mol. Sci. **12**, e1606 (2022).

[56] S. Grimme, S. Ehrlich, and L. Goerigk, Effect of the damping function in dispersion corrected density functional theory, J. Comput. Chem. **32**, 1456 (2011).

[57] F. Weigend, Accurate Coulomb-fitting basis sets for H to Rn, Phys. Chem. Chem. Phys. **8**, 1057 (2006).

[58] R. Sure and S. Grimme, Corrected small basis set Hartree-Fock method for large systems, J. Comput. Chem. **34**, 1672 (2013).